Article:
Capogna, E., Venturi, G., Motta, L. et al. (2026) The role of quantitative susceptibility mapping in dementia with Lewy Bodies. NeuroImage: Clinical, 50. 104000. ISSN: 2213-1582

https://doi.org/10.1016/j.nicl.2026.104000

NeuroImage: Clinical 50 (2026) 104000

Contents lists available at ScienceDirect

NeuroImage: Clinical

journal homepage: www.elsevier.com/locate/ynicl

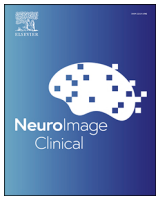

The role of quantitative susceptibility mapping in dementia with Lewy Bodies

Elettra Capogna [a,1], Greta Venturi [a,1], Lorenzo Motta [a], David Neil Manners [a,b], Davide Braghittoni [a], Lucia Guidi [a], Luca Baldelli [c,d], Giovanna Calandra-Buonaura [c,d], Luisa Sambati [d], Annalena Venneri [e,f], Caterina Tonon [a,c,2], Micaela Mitolo [a,e,2], Raffaele Lodi [a,c,2,*]

[a] Functional and Molecular Neuroimaging Unit, IRCCS Istituto delle Scienze Neurologiche di Bologna 40139 Bologna, Italy
[b] Department for Life Quality Studies, University of Bologna, Rimini 47921, Italy
[c] Department of Biomedical and Neuromotor Sciences, University of Bologna 40127 Bologna, Italy
[d] U.O.C. Clinica Neurologica Rete Metropolitana (NeuroMet), IRCCS Istituto delle Scienze Neurologiche di Bologna 40139 Bologna, Italy
[e] Department of Medicine and Surgery, University of Parma 43126 Parma, Italy
[f] Department of Neuroscience, University of Sheffield S10 2HQ Sheffield, UK

ARTICLE INFO

Keywords:
Dementia with Lewy Bodies
Quantitative susceptibility mapping
Substantia nigra
Basal ganglia
Iron overload
DLB early phenotypes

ABSTRACT

Iron overload has been implicated in the pathology of several neurodegenerative diseases, and quantitative susceptibility mapping (QSM), an MRI-based technique, has identified abnormal iron overload in alpha-synucleinopathies. However, there is a limited understanding of the significance of changes in magnetic susceptibility, assessed by QSM, in patients with Dementia with Lewy Bodies (DLB). In this study, 39 DLB patients (58–88 years) and 30 cognitively unimpaired older adults (OA) (56–86 years) underwent an advanced MRI protocol that included T1w and QSM sequences, and a comprehensive neuropsychological evaluation. This study investigated (1) differences in whole-brain magnetic susceptibility and brain volumes between DLB patients and OA; (2) associations between regional changes in magnetic susceptibility and brain volumes, symptom duration, and cognitive functioning; (3) whether regional changes in magnetic susceptibility could differentiate DLB phenotypes based on earlier symptoms. DLB patients showed higher magnetic susceptibility values than OA in the bilateral substantia nigra, globus pallidus, thalamus, brainstem, and hippocampus, as well as in posterior cortical regions. No significant associations were observed between QSM susceptibility values and brain volumes, symptom duration, or cognitive functions. Using classificatory algorithms, different DLB phenotypes were identified based on iron accumulation values in the basal ganglia, thalamus, brainstem, and frontal cortical regions. Our findings suggest that QSM, assessing *in vivo* changes in brain iron accumulation, could serve as a useful noninvasive diagnostic biomarker in DLB patients. Longitudinal studies, including the prodromal phase of DLB, are needed to understand the interplay between brain volumetric loss, iron accumulation, and clinical manifestations.

1. Introduction

Dementia with Lewy bodies (DLB) is the second most common form of dementia (Vann Jones and O'Brien, 2014) and is characterized by the progressive accumulation of aggregated α-synuclein in Lewy bodies and Lewy neurites (McKeith et al., 2017; Outeiro et al., 2019). High inter-individual variability in the spatial pathological accumulation of α-synuclein has been reported in DLB patients, reflecting different neuropathological stages and related clinical symptoms (Jellinger, 2009; Toledo et al., 2016). Disease heterogeneity in DLB is also reflected in different clinical presentations, patterns of cortical and subcortical atrophy, and the presence of concomitant Alzheimer's disease (AD)

* Corresponding author at: Functional and Molecular Neuroimaging Unit, IRCCS Istituto delle Scienze Neurologiche di Bologna, Bologna, Italy.
E-mail address: raffaele.lodi@unibo.it (R. Lodi).
[1] Contributed equally to the study.
[2] Contributed equally to the study.

https://doi.org/10.1016/j.nicl.2026.104000
Received 28 January 2026; Received in revised form 31 March 2026; Accepted 30 April 2026
Available online 1 May 2026

pathology (Ferreira et al., 2021; Inguanzo et al., 2023). Previous studies have attempted to clarify disease heterogeneity in DLB using data-driven clustering approaches based on MRI data, initial clinical presentation of core symptoms, and biological features, and have identified distinct subtypes characterized by different patterns of atrophy, clinical profiles, and progression trajectories (Abdelnour et al., 2022; Inguanzo et al., 2023; Morenas-Rodríguez et al., 2018). Addressing this heterogeneity can improve personalized medicine approaches by refining patient stratification for clinical trials and tailoring therapeutic strategies to specific patient profiles and disease trajectories.

Iron dysregulation has been increasingly implicated in neurodegenerative processes (Ndayisaba et al., 2019) and may contribute to this heterogeneity by differentially affecting brain regions and circuits. Iron overload has been widely studied in AD, Parkinson's disease (PD), and in the prodromal phases of Lewy body disease (LBD), such as REM sleep behavior disorder (RBD), which is considered an early indicator of potential future progression to PD or DLB (De Marzi et al., 2016; Galbiati et al., 2019). However, only a few recent studies have focused on DLB patients (Bhome et al., 2026; Chen et al., 2021; Diaz-Galvan et al., 2025; Kiersnowski et al., 2025). So far, iron dyshomeostasis is thought to be a main contributor or, at least, to play a co-factoring role in the progression of neurodegenerative diseases (Levi et al., 2024; Masaldan et al., 2019; Rouault, 2013). Specifically, in a vicious cycle, iron has been found to interact with the hallmarks of neurodegenerative diseases, such as amyloid-β, tau, and α-synuclein proteins, increasing their production and aggregation (Kostka et al., 2008). In detail, α-synuclein proteins affect iron metabolism and also incorporate iron into their structures, and this interaction promotes protein misfolding and pathological aggregation (Levin et al., 2011; Peng et al., 2010). Moreover, the shift of iron accumulation away from homeostatic levels may increase α-synuclein synthesis and increase aggregate burden (Patel et al., 2018). This imbalance may increase oxidizing capacity, lipid peroxidation, mitochondrial dysfunction, leading to neuronal apoptosis (Ndayisaba et al., 2019). Generally, abnormal iron homeostasis may occur with increasing age (Daugherty and Raz, 2013; Madden and Merenstein, 2023; Ward et al., 2014), regardless of the presence of a specific neurodegenerative condition, with the same outcome: neuroinflammatory processes which involve microglial activation and oxidative stress (Haider et al., 2014; Morris et al., 2018; Wiggermann, 2023), via the production of reactive oxygen species (ROS), which contribute to ferroptosis, an iron-mediated cell death (Masaldan et al., 2019).

Magnetic Resonance Imaging (MRI) can detect changes in tissue magnetic susceptibility based on the paramagnetic or diamagnetic properties of elements and compounds within the brain (Ravanfar et al., 2021), offering a potential non-invasive biomarker of brain iron distribution and accumulation. Indeed, molecules that contain iron have paramagnetic properties including high magnetic susceptibility (Deistung et al., 2017; Duyn and Schenck, 2017). In particular, the MRI-based analysis technique quantitative susceptibility mapping (QSM) is accurate in assessing changes in iron content in gray matter structures, and it has been validated by *post-mortem* studies (Langkammer et al., 2012; Thomas et al., 1993). Furthermore, in neurodegenerative diseases such as DLB, which are characterized by both abnormal iron accumulation and atrophy (Bhome et al., 2026), combining QSM acquisitions and T1w-derived volumes might provide deeper insight into the regional interplay and overlap between volume reduction and iron overload, as well as their timing.

To date, few studies have examined magnetic susceptibility alterations using the QSM technique in DLB patients and have revealed iron deposition in the substantia nigra (Chen et al., 2021; Diaz-Galvan et al., 2025; Kiersnowski et al., 2025). Only one recent study has evaluated whole-brain iron alterations in patients with dementia due to LBD, including both individuals with DLB and individuals with Parkinson's disease dementia (PDD) (Bhome et al., 2026), and has reported increased QSM values across multiple cortical regions compared with cognitively unimpaired participants with PD and healthy controls.

Overall, within the alpha-synucleinopathies (in this context referring to DLB, PD and RBD), abnormal brain iron accumulation has been extensively assessed only in PD and in RBD. An increase in paramagnetic iron concentration has been reported in regions implicated in the neuropathology of the alpha-synucleinopathies, particularly the substantia nigra (including its subregions) and the red nucleus, followed by the basal ganglia, especially the putamen, and globus pallidus nuclei (Mohammadi and Ghaderi, 2024; Ravanfar et al., 2021; Zeng et al., 2024) compared with healthy controls (HC). Indeed, dopaminergic neurons of the substantia nigra contain neuromelanin, which is rich in iron. Moreover, in cognitively unimpaired participants with PD compared with HC, QSM studies showed higher paramagnetic iron concentrations in the hippocampus and thalamus, associated with lower cognitive functioning (Thomas et al., 2020), and in widespread regions of the cortex (Acosta-Cabronero et al., 2017) that were also related to higher dementia risk scores (Thomas et al., 2020). Conversely, RBD patients showed higher concentrations of iron than HC in the substantia nigra, though lower than those observed in patients with PD without dementia (Sun et al., 2020). However, this finding has not been consistently replicated in QSM studies (Lancione et al., 2022). Additionally, higher magnetic susceptibility has been reported in bilateral frontoparietal cortex in RBD compared with HC and PD without dementia (Varga et al., 2024).

Evaluating the presence of an association between cognitive or clinical measures of disease severity and QSM changes helps clarifying the temporal relationship between brain iron accumulation and disease progression. As for global cognitive measures, such as the Mini-Mental State Examination (MMSE) and Montreal Cognitive Assessment (MoCA) scores, several studies have reported no significant correlations with magnetic susceptibility alterations in the substantia nigra (Bhome et al., 2026; Chen et al., 2021; Kiersnowski et al., 2025; Varga et al., 2024). However, no studies have investigated associations between QSM indices and scores on tests assessing specific cognitive domains. As for symptom duration, a positive association between QSM-based iron concentration in the substantia nigra and symptom duration has been reported in some studies (He et al., 2015; Lancione et al., 2022), especially in earlier phases of the disease, although this association has not been consistently replicated (Ghassaban et al., 2019; Varga et al., 2024). No correlation has been reported for other subcortical structures (Ravanfar et al., 2021). It is, therefore, crucial to understand the relationship between brain iron accumulation measured by QSM and different cognitive functions, especially in neurodegenerative conditions in which progressive cognitive decline is observed.

The aim of this study was to assess iron accumulation changes using QSM with a multiple region of interest (ROI) approach that included cortical and subcortical regions in DLB patients compared with cognitively unimpaired older adults (OA). Additionally, we tested whether regional changes in magnetic susceptibility were associated with brain volumes, symptom duration, and cognitive functioning. Lastly, considering the heterogeneity within DLB, we aimed to investigate whether specific QSM-brain features could distinguish DLB phenotypes at the onset of the initial clinical manifestations. We hypothesized that DLB patients would show higher magnetic susceptibility in cortical and subcortical regions, in key structures involved in alpha-synucleinopathies. We further expected that higher susceptibility would be associated with longer symptom duration and lower cognitive scores.

2. Material and methods

2.1. Participants

A total of 69 participants were included in this study: 39 patients with probable DLB (28 males, mean age = 75.64 years, standard deviation [SD] = 6.53) and 30 cognitively unimpaired older adults (OA) (13 males, mean age = 70.64 years, SD = 7.53). DLB patients were enrolled

at the IRCSS Istituto delle Scienze Neurologiche di Bologna, Italy. Inclusion criteria for DLB patients were based on the revised diagnostic criteria from the DLB Consortium for DLB (McKeith et al., 2017), whereas the OA group had no history of neurological disorders and was established to be cognitively healthy following completion of an extensive battery of neuropsychological tests. Additionally, participants were required to have no contra-indications for MR imaging, no history of psychiatric disorders or substance abuse, no excessive daytime sleepiness as assessed by the Epworth Sleepiness Scale (ESS score > 10) (Johns, 1991), no use of medications known to affect nervous system functioning and pupillary light reflex, no moderate or severe cerebral small vessel disease or focal brain lesions. Specific inclusion criteria for the OA group and biomarkers for the characterization of DLB patients are listed in the Supplementary Info (**SI**). A subsample of DLB patients (n = 20) were also tested for core cerebrospinal fluid (CSF) AD biomarkers (data reported in the **SI**).

All participants underwent the same brain MRI protocol, described below, and a comprehensive clinical and neuropsychological assessment.

The neuropsychological battery included assessments of different cognitive domains with the following tests: memory (Digit Span forward, Corsi block-tapping test, Rey Auditory Verbal Learning test immediate and delayed, and Rey-Osterrieth complex figure recall) (Caffarra et al., 2002; Carlesimo et al., 1996; Monaco et al., 2013), executive functions (Digit span backward, phonemic fluency, Stroop test time and errors) (Caffarra et al., 2002; Carlesimo et al., 1996; Monaco et al., 2013), visuoperceptual/visuospatial functions (Rey-Osterrieth complex figure copy, Benton Judgment of Line Orientation test and Visual Object and Space Perception Battery-VOSP) (Caffarra et al., 2002; Ferracuti et al., 2000; Warrington and James, 1991), and language (semantic fluency) (Zarino et al., 2014). All participants gave written informed consent, and the study was approved by the local ethical committee (#CE 20225, Comitato Etico di Area Vasta Emilia Centro, AVEC) and conducted in accordance with the Declaration of Helsinki.

Furthermore, patients were categorized into an early cognitive/psychiatric phenotype and an early RBD/motor phenotype based on their initial clinical presentation as recorded in their medical records. More specifically, DLB patients were labeled as early cognitive/psychiatric phenotype (n = 16, mean age = 76.24 years, SD = 7.34) if at onset manifested cognitive dysfunction or psychiatric symptoms, such as depression, apathy, anxiety, hallucinations, and delusions. Twenty-three out of 39 DLB patients were classified as early RBD/motor phenotype given that their earliest symptoms at onset were extrapyramidal motor symptoms or RBD (mean age = 75.13 years, SD = 6.37). See Supplementary Table 1 for a clinical characterization of the DLB early phenotypes.

2.2. MRI acquisition

Imaging data were collected using a Siemens Head/Neck 64 Coil on a 3 T clinical MRI scanner (Magnetom Skyra, Siemens Healthineers, Erlangen, Germany) at the IRCSS Institute of Neurological Sciences, Bologna, Italy. The MRI acquisition protocol included Magnetization Prepared Rapid Acquisition Gradient Echo (MPRAGE) (3D T1w, sagittal, TE/TR = 53/2300 ms, TI = 900 ms, FA = 9°, 1 × 1 × 1 mm^3, duration ~ 5′) and QSM (3D GRE T2*w, axial, TE1/ΔTE/TR = 9.42/9.42/53 ms, FA = 15°, 0.5 × 0.5 × 1.5 mm^3, duration ~ 9′) sequences. Moreover, for clinical purposes, the following sequences were also acquired: Fluid-Attenuated Inversion Recovery (FLAIR) (3D T2w, sagittal, TE/TR = 428/5000 ms, FA = 120°, 1 × 1 × 1 mm^3, duration ~ 6′) and a multishell Diffusion Tensor Imaging sequence: b = 0 (n = 8 AP/PA), 300 (n = 8 AP/PA), 1000 (n = 30 AP/PA), 2000 s/mm^2 (n = 64 AP), duration ~ 13′).

2.3. QSM and MRI processing

Phase maps acquired at five different echo times using a T2*w sequence were individually processed through Laplacian phase unwrapping (Schweser et al., 2011), followed by background field removal using the Variable-kernel Sophisticated Harmonic Artifact Reduction for Phase data (V-SHARP) method (Li et al., 2011). A brain mask was obtained by applying the FSL Brain Extraction Tool (Biondetti et al., 2022) (BET) to the magnitude image of the first echo. The processed phase maps were then combined into a single-phase image using a weighted averaging approach (Biondetti et al., 2022), where the weights were defined as:

$$w(TE_i) = \frac{TE_i e^{-TE_i/T_2^*}}{\sum_{j=1}^{5} TE_j e^{-TE_j/T_2^*}}$$

Dipole inversion was performed using the iterative Least Squares QR (iLSQR) method (Li et al., 2015). The entire QSM pipeline was implemented using the STI Suite toolbox (https://people.eecs.berkeley.edu/~chunlei.liu/software.html). The resulting susceptibility maps were linearly registered to the corresponding T1-weighted structural images using FLIRT (FSL).

CSF was used as the reference tissue by applying the zero-referencing method (Straub et al., 2017). Since QSM signal in the ventricles is often non-uniform due to the presence of blood vessels and partial volume effects, we selected three small and anatomically distinct CSF volumes: the anterior horns, the body, and the atrium of the lateral ventricles (Wang and Liu, 2015). These regions are considered stable across subjects and less affected by susceptibility orientation dependence or age-related changes (Committee et al., 2024). An atlas-based approach was implemented to identify automatically these CSF regions across subjects. This atlas was constructed using data from 60 individuals (Fiscone et al., 2024), combining linear registration between QSM and MPRAGE images within each subject with a non-linear registration (FNIRT, FSL) of individual MPRAGE scans to a common template space. The CSF reference ROIs were manually defined in the atlas space and then back-registered to each subject's native QSM map to extract the mean susceptibility values. The final susceptibility maps (Fiscone et al., 2024, 2023) were expressed in parts per million (ppm), with a typical dynamic range between approximately –0.2 and 0.2 ppm.

T1-weighted MPRAGE images were segmented using FreeSurfer (version 6.0) (Fischl et al., 2002), which performs automated surface reconstruction and anatomical labeling. Cortical segmentation was based on the Desikan-Killiany atlas (Desikan et al., 2006), resulting in 34 labeled cortical gyri per hemisphere. Subcortical segmentation was also performed using FreeSurfer, identifying the following regions of interest: thalamus, caudate, putamen, globus pallidus, brainstem, hippocampus, amygdala, and accumbens area. For each cortical and subcortical structure, left and right segmentations were merged into a single bilateral ROI to increase measurement robustness. Brainstem structures were further segmented using the FreeSurfer dedicated brainstem module (Iglesias et al., 2015) that provides finer delineation of the midbrain, pons, and medulla. Moreover, our aim was to focus on targeted brain structures implied in alpha-synucleinopathies. Hence, to improve anatomical accuracy within deep gray matter nuclei, especially the basal ganglia, a high-resolution probabilistic atlas based on ultra-high field 7 T MRI data (Keuken and Forstmann, 2015) was used. The atlas includes the striatum, internal and external segments of the globus pallidus, subthalamic nucleus, substantia nigra, periaqueductal gray, and red nucleus, and was non-linearly registered to each subject's anatomical space using the FSL FNIRT tool. In regions where segmentations at the substructure level were included, such as the brainstem and globus pallidus, a unified ROI was obtained by summing their respective subcomponents.

After segmentation, QSM images were linearly registered to the corresponding T1-weighted MPRAGE images using the FSL FLIRT tool (Jenkinson and Smith, 2001) to map anatomical ROIs onto the susceptibility maps. From each ROI, both volume and median magnetic susceptibility values (Yao et al., 2023) were extracted.

2.4. Statistical analysis

All variables were tested for normality using the Shapiro-Wilk test. Sociodemographic and neuropsychological data were compared across groups, using ANOVA and Mann-Whitney U tests, according to data distribution. For the neuropsychological variables, sex, age, and education were included as covariates of no interest. Differences in sex were assessed using a chi-square test.

Parametric (ANOVA) or non-parametric (Mann–Whitney U) tests were applied to investigate differences between patients and OA in QSM and T1w-derived volumetric values in each cortical and subcortical ROI. The QSM values in all ROIs used in these tests were corrected for age, while brain volumes were adjusted for sex, age, and estimated total intracranial volume (eTIV) using a residual approach. Specifically, within the OA group, linear regression models were fitted for each region of interest, and the resulting coefficients were used to compute adjusted values for all subjects (Kiersnowski et al., 2025). The results were corrected for multiple comparisons using the Benjamini–Hochberg false discovery rate (FDR) (Benjamini and Hochberg, 1995), at the level of the single modality. Next, to understand whether iron deposition was related to neuronal loss, we assessed the association between regional QSM and T1w-derived volume values across groups using a partial Spearman correlation, correcting for age, sex, and eTIV.

Moreover, in the DLB group, we also tested the correlation between regional QSM values and symptom duration (i.e., the time between symptom onset and study enrollment), controlling for age. Due to inconsistent findings regarding the relationship between magnetic susceptibility values and symptom duration in neurodegenerative conditions (Ravanfar et al., 2021), we also tested whether the effect of symptom duration should be included as a covariate in our QSM analyses. Finally, the relationship between regional magnetic susceptibility indices and cognitive scores where significant group differences had been identified by comparisons with OA was analyzed using a partial Spearman correlation, adjusting for sex, age, and education. The results were corrected for multiple comparisons using the Benjamini–Hochberg FDR.

All statistical analyses were performed using custom Python 3.11 scripts and R environment version 4.5.0. Results were categorized as significant ($p < 0.05$), highly significant ($p < 0.01$), or extremely significant ($p < 0.001$).

2.5. DLB early predominant phenotype classification: subgroup comparison of regional changes in magnetic susceptibility and cognitive functioning, and QSM-based prediction

We assessed whether the early cognitive/psychiatric phenotype and early RBD/motor phenotypes differed in sociodemographic variables (sex, age, and education), symptom duration, cognitive functioning and brain QSM patterns using ANOVA and Mann-Whitney U tests. The QSM values in all ROIs were corrected for age. Cognitive tests were adjusted for age, sex, and education. FDR correction was applied to the models.

A supervised machine learning approach (specifically, a logistic regression model) was used to classify patients into one of two previously identified early phenotypes based on regional magnetic susceptibility values. The input features for the model were QSM values from individual ROIs, which had been adjusted for age using a residual-based approach. The training pipeline included z-score normalization and univariate feature selection (Costanzo and Orphanou, 2022). The top 10 most discriminative features were selected using an ANOVA F-test criterion. Model performance was evaluated using stratified 5-fold cross-validation to preserve class balance across training and test sets. At each fold, classification metrics including accuracy, precision, recall, and F1-score were computed using macro-averaging. Normalized confusion matrices were also generated to assess classification reliability across subtypes. This framework enabled the identification of QSM-derived features most relevant for distinguishing DLB early phenotypes.

3. Results

3.1. Cohort characteristics

The baseline characteristics of the cohorts are presented in Table 1. No significant group differences were observed for sex and education ($pFDR > 0.05$), whereas the groups differed significantly in age. Age was included as a covariate in all analyses (Dukart et al., 2011; Falahati et al., 2016). As expected, DLB patients scored lower than the OA participants on the MMSE and on most of the neuropsychological tests.

3.2. Cortical and subcortical magnetic susceptibility and volume differences between DLB and OA

A widespread pattern of abnormal cortical magnetic susceptibility was found in DLB patients compared with OA. These patients showed higher magnetic susceptibility values in the occipito-temporal regions and in the posterior and anterior parietal regions, including the supramarginal gyrus ($F = 5.43$, $pFDR = 0.04$), precuneus ($F = 5.40$, $pFDR = 0.04$), and postcentral gyrus ($F = 5.81$, $pFDR = 0.04$). Additionally, DLB patients exhibited higher susceptibility in orbitofrontal regions compared with OA (lateral orbitofrontal region [$F = 7.27$, $pFDR = 0.04$], and medial orbitofrontal [$F = 8.53$, $pFDR = 0.03$] respectively). When assessing brain volume differences, DLB presented more cortical atrophy compared with OA, particularly in occipitoparietal regions (lingual [$F = 5.28$, $pFDR < 0.05$], lateral occipital [$F = 4.85$, $pFDR < 0.05$], precuneus [$F = 5.21$, $pFDR < 0.05$], inferior parietal [$F = 4.76$, $pFDR < 0.05$],) and in the superior and inferior frontal regions. Fig. 1 presents the cortical regions in which significant differences were found, while Supplementary Table 2 gives an overview of all the models.

In subcortical regions, DLB patients exhibited higher magnetic susceptibility in the substantia nigra ($F = 11.16$, $pFDR < 0.01$), and across the entire brainstem ($F = 11.04$, $pFDR < 0.01$) and its substructures, such as the midbrain ($F = 15.86$, $pFDR < 0.01$), the pons ($F = 11.57$, $pFDR < 0.01$), and the medulla ($F = 12.51$, $pFDR < 0.01$), when compared with OA. Furthermore, higher magnetic susceptibility was observed in the globus pallidus ($F = 7.55$, $pFDR = 0.02$) and its subdivisions (external [$F = 6.20$, $pFDR = 0.03$], and internal [$F = 8.72$, $pFDR = 0.01$]), as well as in the thalamus ($F = 5.30$, $pFDR = 0.05$), and hippocampus ($F = 6.24$, $pFDR = 0.03$).

When comparing DLB and OA in terms of brain volumes, we found that DLB patients showed greater volumetric loss, resulting in smaller volumes in the amygdala ($F = 15.99$, $pFDR < 0.01$) and in the hippocampus ($F = 10.27$, $pFDR = 0.02$). The hippocampus was the sole region in which both volume reduction and higher magnetic susceptibility values were observed, whereas other regions, particularly in the basal ganglia, such as the globus pallidus and the substantia nigra (midbrain), presented higher magnetic susceptibility values, likely reflecting iron accumulation. Results for the subcortical regions are presented in Fig. 2, while Supplementary Table 3 gives an overview of all the models.

3.3. Correlations between regional magnetic susceptibility, brain volume, and symptom duration

Considering the potential link between iron deposition and atrophy in both cortical and subcortical regions, we tested the relationship between regional magnetic susceptibility and brain volumes across groups. After pFDR correction, we found no significant associations between regional magnetic susceptibility and brain volumes except for the nucleus accumbens ($\rho = 0.61$, $pFDR = 0.01$). Consequently, we decided not to include brain volumes as a covariate of interest in our QSM analyses. The same approach was applied to assess the effect of symptom duration. Indeed, no significant correlation was found between susceptibility values and symptom duration in any of the cortical and subcortical structures of DLB patients, after correction for multiple comparisons ($pFDR > 0.05$). The results of all the correlation analyses are reported in

Table 1
Cohort characteristics.

	DLB	OA	Cohort differences (pFDR)	Effect size
Characteristics				
N (F:M)	39 (11:28)	30 (17:13)	3.4 (0.06)	0.22
Age (years)	75.64 (6.53)	70.64 (7.53)	8.9 (0.01)*	0.71
Age range	58–88	56–86		
Education (years)	11.50 (3.26)	10.95 (3.75)	543.5 (0.40)	0.10
Symptom duration (years)	7.37 (4.30)	–	–	–
MMSE	23.80 (5.32)	29.36 (0.87)	30.43 (<0.001)*	−1.32
Memory domain				
Digit Span forward	4.98 (1.06)	5.60 (1.04)	2.0 (0.16)	−0.34
Corsi block-tapping test	3.80 (1.25)	5.03 (0.81)	15.9 (<0.001)*	−0.96
RAVLT immediate	25.10 (12.54)	45.07 (9.48)	27.76 (<0.001)*	−1.27
RAVLT delayed	4.28 (3.41)	9.80 (3.02)	201 (<0.001)*†	0.56
ROCF recall	8.05 (6.11)	19.66 (5.11)	123 (<0.001)*†	0.68
Executive functions domain				
Digit span backward	3.34 (0.99)	4.03 (0.72)	7.56 (<0.01)*	−0.66
Phonemic fluency	24.20 (15.82)	39.83 (14.21)	12.1 (0.001)*	−0.83
Stroop test time	40.53 (31.44)	19.80 (8.58)	9.49 (<0.01)*	0.76
Stroop test errors	6.80 (8.89)	0.23 (0.77)	16.18 (<0.001)*	0.99
Language domain				
Semantic fluency	25.37 (9.33)	45.40 (10.25)	56.77 (<0.001)*	−1.81
Visuoperceptual/ visuospatial functions domain				
ROCF copy	22.77 (11.40)	34.73 (1.93)	29.99 (<0.001)*	−1.31
BJLOT	17.74 (8.30)	24.80 (3.18)	258 (<0.001)*†	0.48
VOSP shape detection screening test	18.85 (1.31)	19.53 (0.68)	3.51 (0.07)	−0.45
VOSP incomplete letters	15.43 (5.40)	19.53 (0.68)	168 (<0.001)*†	0.61
VOSP silhouettes	13.75 (4.28)	20.57 (3.35)	42.95 (<0.001)*	−1.58
VOSP object decision	13.28 (3.19)	17.17 (1.55)	37.86 (<0.001)*	−1.49
VOSP progressive silhouettes	12.70 (2.46)	9.87 (2.61)	9.81 (<0.01)*	0.76
VOSP dot counting	9.15 (1.73)	9.90 (0.31)	262 (<0.001)*†	0.48
VOSP position discrimination	18.20 (2.71)	19.90 (0.40)	10.42 (<0.01)*	−0.78
VOSP number location	7.38 (2.71)	9.53 (0.82)	16.23 (<0.001)*	−0.97
VOSP cube analysis	6.83 (2.41)	9.83 (0.38)	44.21 (<0.001)*	−1.60

Descriptive statistics represent mean (SD). N = number of subjects. DLB = Dementia with Lewy Bodies, OA = cognitively unimpaired older adults, MMSE = Mini Mental State Examination, RAVLT = Rey Auditory Verbal Learning test, ROCF = Rey-Osterrieth complex figure, BJLOT = Benton Judgment of Line Orientation test, VOSP = Visual Object and Space Perception Battery. Cohort differences are assessed using chi-squared test for dichotomous variables. Based on the data distribution, parametric (ANOVA) or non-parametric (Mann–Whitney U) tests were used. Effect size for cohort differences is assessed using Cohen's D for continuous variables and Cramer's V for dichotomous. For non-parametric Mann–Whitney U tests (marked with †), the effect size r was calculated using the formula $r = \frac{|Z|}{\sqrt{N}}$, where Z is the standardized U statistic and N is the total sample size. False discovery rate (pFDR) correction was applied to the models.

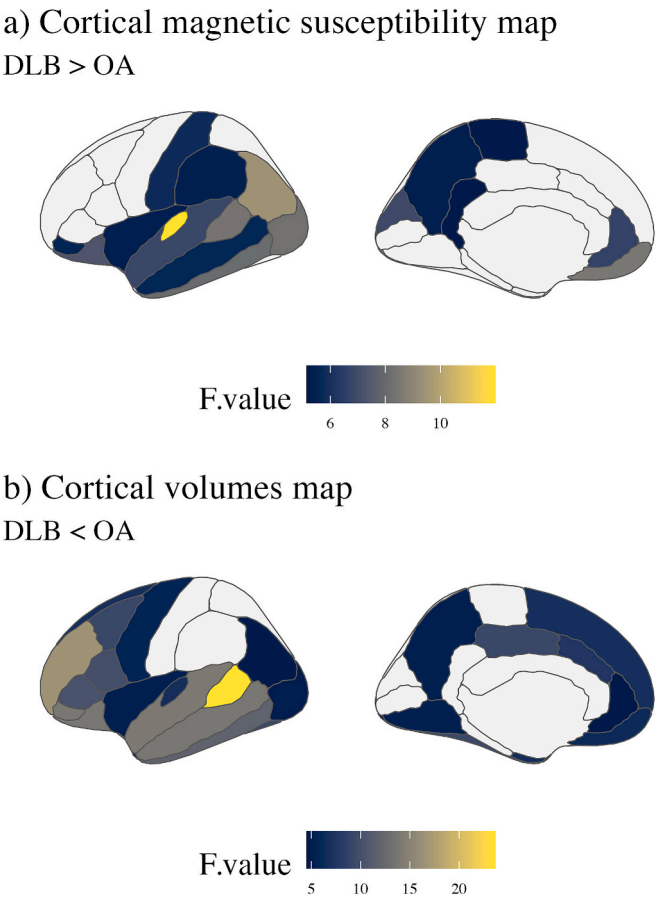

Fig. 1. Significant brain cortical susceptibility and volume differences between DLB and OA. ANOVA output of cortical differences. Color-coded F-values are shown for regions surviving FDR correction (pFDR < 0.05); non-significant regions are shown in white. Yellow represents higher magnetic susceptibility (higher volumetric loss) and blue lower magnetic susceptibility (lower volumetric loss) values. ROIs were based on the Desikan-Killiany atlas (Desikan et al., 2006). DLB = Dementia with Lewy Bodies, OA = cognitively unimpaired older adults. A) Cortical magnetic susceptibility differences (DLB > OA), controlling for age. B) Cortical volume differences (DLB < OA), controlling for sex, age, and total intracranial volume. (For interpretation of the references to colour in this figure legend, the reader is referred to the web version of this article.)

[Zenodo] at https://doi.org/10.5281/zenodo.18324266 and in Supplementary Table 4.

3.4. Associations between regional magnetic susceptibility and cognitive functioning

No significant relationship was observed between the magnetic susceptibility of significant subcortical or cortical regions and cognitive scores on those tests for which a significant difference from OA's scores had been identified, following correction for multiple comparisons.

At the trend level for the visuoperceptual/visuospatial domain, we observed negative associations between the VOSP silhouettes subtest and several frontal regions (uncorrected p < 0.005), occipital regions including the cuneus (ρ = -0.39) and lateral occipital cortex (ρ = -0.36),

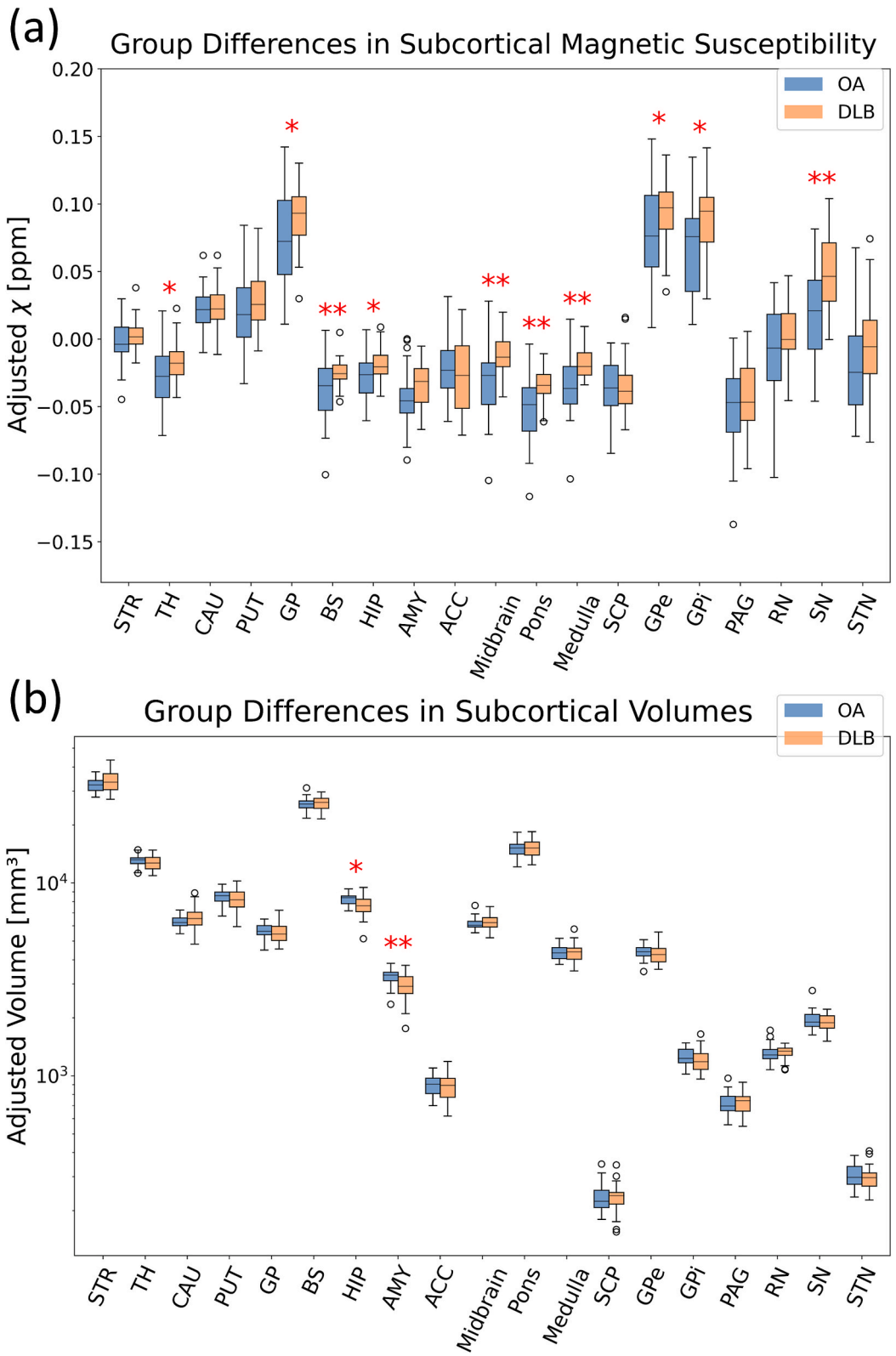

Fig. 2. Significant subcortical magnetic susceptibility and volume differences between DLB and OA. A) Median magnetic susceptibility values in subcortical regions across groups. Adjusted χ refers to the magnetic susceptibility values, corrected for age by residualization based on a linear fit of susceptibility against age in the OA group. B) Mean volume values in subcortical regions across groups. All brain volumes were adjusted for sex, age, and estimated total intracranial volume (eTIV) using a residual approach. STR = striatum, TH = thalamus, CAU = caudate, PUT = putamen, GP = globus pallidus, BS = brainstem, HIP = hippocampus, AMY = amygdala, ACC = nucleus accumbens, SCP = superior cerebellar peduncle, GPe = globus pallidus external, GPi = globus pallidus internal, PAG = periaqueductal gray, RN = red nucleus, SN = substantia nigra, STN = subthalamic nucleus. DLB = Dementia with Lewy Bodies, OA = cognitively unimpaired older adults. * indicates pFDR < 0.05, ** indicates pFDR < 0.01. (For interpretation of the references to colour in this figure legend, the reader is referred to the web version of this article.)

as well as middle temporal regions ($\rho = -0.35$) (uncorrected $p < 0.05$). Hence, higher magnetic susceptibility in these regions was associated with poorer performance on the VOSP subtest. We report all the correlations between the cognitive scores and regional QSM values in [Zenodo] at https://doi.org/10.5281/zenodo.18324266.

3.5. DLB early predominant phenotype classification based on QSM-brain features

We assessed whether the early cognitive/psychiatric phenotype vs early RBD/motor phenotype categorical subgroups differed in sociodemographic variables, symptom duration, cognitive functioning and brain QSM patterns. No models survived correction for multiple comparisons. Comprehensive statistics of the univariate comparisons can be found in Supplementary Table 5.

The logistic regression model, trained with the top 10 features selected through ANOVA F-test, yielded an average classification accuracy of 0.73 ± 0.04 across stratified 5-fold cross-validation. Macro-averaged precision was 0.73 ± 0.09, F1-score was 0.69 ± 0.07, recall was 0.71 ± 0.05, indicating consistent performance across classes. The average normalized confusion matrix (Fig. 3a) showed that 79.2% of early RBD/motor phenotype cases were correctly classified, whereas 62.6% of early cognitive/psychiatric phenotype cases were accurately identified. The most predictive features (Fig. 3b) for cortical regions, in descending order, were: paracentral, medial orbitofrontal, post central, pericalcarine, and insula. For subcortical regions, the most significant features were medulla, pons, nucleus accumbens, substantia nigra, and thalamus. These features demonstrated the highest F-scores in the univariate selection, highlighting their relevance in distinguishing an early cognitive/psychiatric phenotype from an early RBD/motor phenotype based on QSM measurements.

Overall, although univariate comparisons did not reveal statistically significant group differences, the multivariate logistic regression model (trained on the top 10 features) differentiated between the early cognitive/psychiatric and early RBD/motor phenotypes. These findings suggest that the distinction between subtypes is not driven by isolated regional abnormalities, but rather by a spatial pattern of QSM alterations involving both cortical and subcortical structures. Such patterns may reflect differences in regional brain vulnerability, consistent with the heterogeneous nature of DLB.

4. Discussion

Higher magnetic susceptibility detected using the QSM technique in key subcortical and cortical regions associated with DLB, which allowed differentiation of DLB early predominant phenotypes, is the main and novel findings of this study. Specifically, DLB patients displayed higher magnetic susceptibility values, likely reflecting iron accumulation in the substantia nigra, globus pallidus, brainstem, thalamus, and hippocampus, as well as in posterior cortical regions (occipitotemporal and occipitoparietal) and in orbitofrontal regions. A widespread pattern of cortical atrophy was also observed in DLB patients, especially in frontal and occipito-parietal regions, and, to a lesser degree in subcortical structures, with only the amygdala and hippocampus showing significant volume loss. This might suggest different neurobiological mechanisms underlying volume loss and abnormal iron concentration at both subcortical and cortical levels in this clinical population. Moreover, it was possible to distinguish the two DLB early predominant phenotypes (early cognitive/psychiatric and early RBD/motor phenotypes) based on the magnetic susceptibility values detected in the brainstem, substantia nigra, basal ganglia, insula, and frontal regions.

At the subcortical level, our findings of higher magnetic susceptibility in the substantia nigra among DLB patients align with previous studies in this population (Chen et al., 2021; Diaz-Galvan et al., 2025) and with observations in PD and PDD patients (Bhome et al., 2026; Fu et al., 2021; Lancione et al., 2022). The temporal relationship between α-synucleinopathy and iron accumulation remains challenging. A recent study (Diaz-Galvan et al., 2025) found that increased abnormal iron accumulation in the substantia nigra was observed in individuals with Lewy body pathology at autopsy, suggesting that QSM might be useful as an *in vivo* biomarker in the context of Lewy body-related pathology.

Among other basal ganglia structures, we found higher magnetic susceptibility in the globus pallidus, both in the external and internal region, as well as in the thalamus. This finding is consistent with other studies in PD patients (Chen et al., 2019; Langkammer et al., 2016; Shahmaei et al., 2019) in which iron accumulation in the globus pallidus has been related to longer symptom duration. Based on a circuit-level framework, we hypothesize that higher iron deposition within key output nodes of the basal ganglia, such as the globus pallidus and the substantia nigra, may contribute to altered basal ganglia-thalamocortical signaling (McGregor and Nelson, 2019). These structures exert a strong inhibitory influence on thalamic activity and their dysfunction may therefore impact the regulation of thalamocortical

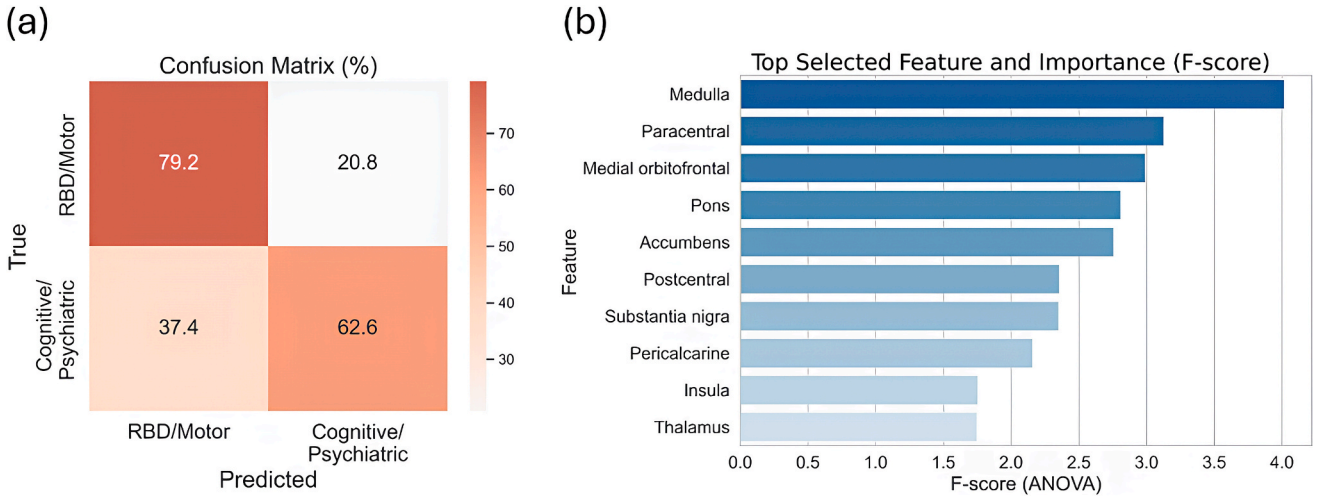

Fig. 3. DLB phenotype classification. (a) Confusion matrix (average values in %) for the logistic regression model using the top 10 features. Rows indicate true classes and columns indicate predicted classes. The model shows higher accuracy in classifying body-first than brain-first DLB cases. (b) Bar plot of the top 10 most discriminant features ranked by F-score, based on univariate feature selection (ANOVA F-test). Features include cortical and subcortical brain regions derived from QSM data, adjusted for age and symptom duration.

integration within motor networks, potentially contributing to some of the extrapyramidal symptoms observed in our sample, as reported in the patients' medical records. However, we were unable to test this association empirically using a structured assessment of motor symptoms. Given this limitation, the need for further investigations remains.

We also found higher magnetic susceptibility in the brainstem, including the midbrain, pons, and medulla. It has been suggested that RBD, commonly experienced by DLB patients (McKeith et al., 2017), involves changes in brainstem structures, especially due to the initial pathological accumulation of α-synuclein in the pons (Joza et al., 2023; Miglis et al., 2021) and in the nigrostriatal dopaminergic system (Nepozitek et al., 2023; Zoetmulder et al., 2016). In our study within the early RBD/motor phenotype, 57% of patients also showed presynaptic dopaminergic dysfunction in the nigrostriatal pathway, when assessed by DAT-SPECT (data reported in SI). We can speculate that increased iron accumulation in the brainstem (particularly in the pons and the substantia nigra) and basal ganglia might be associated with the presence of extrapyramidal motor symptoms or RBD, which were observed as early clinical manifestations in approximately 59% of our DLB patients (early RBD/motor phenotype). Moreover, most participants in our overall sample experienced these symptoms at the time of QSM acquisition, even if their earlier presentation was not consistent with an RBD/motor onset phenotype.

We also found abnormal magnetic susceptibility values in the hippocampus, as previously reported in PD and PDD patients (Acosta-Cabronero et al., 2017; Bhome et al., 2026). Moreover, the hippocampus was the only subcortical region where volume reduction was also found. Abnormal iron accumulation and brain atrophy, both markers of neuronal damage (Dixon and Stockwell, 2014), have also been reported in the medial temporal lobe (MTL) in α-synucleinopathies (Weintraub et al., 2012). Although relative preservation of the MTL is considered a supportive biomarker for a diagnosis of DLB (McKeith et al., 2017), recent reviews (Barba et al., 2024; Chin et al., 2020) have reported that up to 25–40% of patients with DLB may also present with AD neuropathological changes, which may impact hippocampal volume, especially due to tau pathology. This result is further corroborated by neuropathological studies (Irwin et al., 2017) in dementia due to LBD that confirmed a strong association between AD neuropathological changes and α-synuclein, noting that they increase together, especially with increasing age, and in the later stages of the disease there is greater probability of co-pathology (Ferreira et al., 2020). Atrophy of the hippocampus and amygdala has also been reported in DLB patients (Khadhraoui et al., 2022), and it has been found associated with the severity of cognitive symptoms (Elder et al., 2017). Presence of co-pathology could suggest a more advanced stage of disease and explain the pattern of cognitive decline of our sample that involved several domains, including long-term memory. In this context, memory decline may emerge at later stages of disease progression, in addition to earlier detectable impairments in attention, executive functions, and visuoperceptual/visuospatial processing that normally characterize the earliest stages of disease.

At the cortical level, we observed higher magnetic susceptibility in occipitotemporal and occipitoparietal regions. This observation is consistent with the findings of studies of DLB patients that have used other neuroimaging techniques (e.g., FDG-PET and functional MRI) and have reported posterior hypometabolism, associated with impairment of visuoperceptual and visuospatial functions (Beretta et al., 2022, 2019), and increased activity related to visual hallucinations (Ffytche et al., 1998; Zorzi et al., 2021). We can speculate that higher magnetic susceptibility in these regions might explain psychiatric and cognitive symptoms that were observed as early clinical features in approximately 41% of our DLB patients (early cognitive/psychiatric phenotype). Notably, multidomain cognitive symptoms were present in all our DLB participants at the time of QSM acquisition. Our QSM results partially aligns with another study that compared DLB and PDD patients with cognitively unimpaired PD and HC, revealing higher iron accumulation in temporal regions (Bhome et al., 2026).

Although to a lesser extent than in patients with AD, overall cortical atrophy in posterior and frontal regions is also observed in DLB patients (Oppedal et al., 2019), a finding also detected in our study.

Parietal regions such as the precuneus and inferior parietal cortex exhibited both higher magnetic susceptibility values, likely reflecting iron accumulation and volumetric loss, in our sample.

Overall, in our cross-sectional sample, subcortical regions exhibited abnormal iron accumulation and relative sparing of volume, whereas cortical regions showed more atrophy. Cuneus, supramarginal and primary somatosensorial areas were the only cortical regions spared from volumetric loss although showing higher magnetic susceptibility values, likely reflecting iron accumulation.

Higher susceptibility in cortical and subcortical regions was not significantly correlated with volumetric loss, nor with symptom duration. This pattern of findings in our sample makes the understanding of the interplay between brain atrophy and iron accumulation challenging. In our sample, there were areas solely impacted by volume reduction, regions influenced only by iron accumulation, and others where both pathological processes were detected. This pattern aligns with the findings of a recent study in patients with dementia due to LBD (Bhome et al., 2026) in which no overlap between these pathological processes was found in posterior parietal regions, where only gray matter reduction without iron accumulation was observed, indicating potentially distinct neurobiological processes. Notably, significant abnormal magnetic susceptibility values were independent of atrophy (when analyses were corrected for it), consistent with our findings.

The lack of a longitudinal assessment, tracking patients from the prodromal to late phases of disease prevents clarification of QSM and volume change trajectories, making it impossible to determine whether iron changes precede volume changes or vice versa. Moreover, we cannot determine whether iron levels continue to increase before or after atrophy reaches a plateau. The exact mechanisms underlying QSM changes remain unclear: alterations in magnetic susceptibility values can result from either an absolute iron accumulation or a relative increase in iron concentration due to atrophy (Duyn and Schenck, 2017).

As for cognition, we found no significant relationship between magnetic susceptibility values and cognitive scores. We only found a trend between higher magnetic susceptibility in occipito-temporal and frontal regions and poorer performance on the VOSP silhouettes subtest. A few studies have examined the relationship between QSM changes and cognitive impairment in pathological conditions, and the results are not univocal. Most studies have reported no significant associations in patients with DLB, PDD, RBD, PD, and prodromal DLB patients (Bhome et al., 2026; Chen et al., 2021; Kiersnowski et al., 2025; Varga et al., 2024), or in AD patients (Moon et al., 2016). There is, however, a small number of studies in PD patients that have reported a negative relationship between QSM values in the caudate nucleus and hippocampus, and MoCA scores (Thomas et al., 2020; Uchida et al., 2020), as well as between QSM values in other basal ganglia structures and the MDS-UPDRS-I for non-motor symptoms (Langkammer et al., 2016). Lack of a significant association between iron accumulation and cognitive decline in our study might be due to the fact that iron accumulation might represent one of the earliest changes in disease progression and may not have a linear relationship with cognitive decline in the symptomatic phase of neurodegenerative disorders (Moon et al., 2016). Evidence from other neurodegenerative conditions indicates that iron deposition may increase during prodromal or early symptomatic phases and subsequently slow or reach a plateau at later stages of the disease (Du et al., 2022), where more severe cognitive deficits are observed. In patients with established DLB, iron levels may therefore already be relatively stable, limiting the possibility of detecting cross-sectional associations with symptom duration or cognitive scores.

We applied a supervised machine learning approach to identify the most informative brain regions (in terms of changes in magnetic susceptibility) that could successfully differentiate DLB phenotypes (based

on the earliest experienced symptoms). Our algorithm demonstrated moderate accuracy, particularly with a higher classification rate for DLB patients with RBD or extrapyramidal symptoms as earlier clinical presentations (early RBD/motor phenotype). Regional changes in magnetic susceptibility that best explained our classification were located in primary sensorimotor and visual cortices (paracentral, postcentral, pericalcarine), frontolimbic areas and components of the olfactory processing network (medial orbitofrontal cortex, insula), subcortical and brainstem structures (substantia nigra, thalamus, nucleus accumbens, pons, and medulla). Given the non-directional nature of this analysis, abnormal iron accumulation in these regions can be interpreted as not specifically associated with a single symptom domain. These areas likely highlight widespread neuroanatomical patterns that together are differentially informative in capturing early clinical presentation of DLB. For instance, using a clustering approach on brain volumes, Iguanzo et al. (2023) pinpointed the regions that contributed most significantly to the identification of DLB subtypes, which included the pons and the olfactory cortex, similar to the findings in our study. Importantly, these neuroimaging-defined subtypes did not differ substantially in symptom duration or core clinical features, suggesting that they primarily reflect differences in neuroanatomical vulnerability rather than distinct clinical entities. Another study (Morenas-Rodríguez et al., 2018) identified three clinical phenotypes in DLB patients based on the initial clinical manifestations: cognitive predominant, neuropsychiatric with more psychotic symptoms and parkinsonism predominant. Differences in the initial clinical presentation might stem from variability in regional pathological α-synuclein accumulation (Ferman et al., 2020). For instance, greater disruption of brainstem integrity might lead to more pronounced motor features or RBD, whereas a primarily cortical distribution might result in psychiatric and cognitive disturbances (Colom-Cadena et al., 2017; Morenas-Rodríguez et al., 2018). So far, multiple classification frameworks for DLB have been proposed including clinical, neuropsychological, neuroanatomical, pathogenic (body-first vs brain-first), molecular, network-based, genetic models (Abdelnour et al., 2022; Borghammer et al., 2021; Horsager and Borghammer, 2024; Inguanzo et al., 2023; Morenas-Rodríguez et al., 2018). These frameworks are largely complementary rather than mutually exclusive and likely capture different dimensions of disease heterogeneity.

In our case, higher magnetic susceptibility values, likely reflecting iron accumulation in the brainstem, basal ganglia, thalamus, insula, and frontal regions contributed to the differentiation of early RBD/motor and early cognitive/psychiatric phenotypes in our DLB sample. The pathological involvement of these regions might explain the heterogeneity in early clinical presentation of the disease. However, although suggestive, based on our results, we cannot determine the temporal relationship between abnormal iron and α-synuclein accumulation, and clinical symptoms, nor can we confirm the presence of Lewy body pathology in these regions in our sample. Moreover, in our study, patients were not characterized in the prodromal stages of the disease, suggesting they were likely at a more advanced stage at the time of QSM acquisition. By this stage, neurodegeneration and alpha-synuclein pathology had plausibly already spread to key regions, making it difficult to differentiate patients based on presenting symptoms. Although these results should be interpreted with caution given the relatively limited sample size, they provide proof of concept that regional susceptibility patterns may capture biologically meaningful aspects of early clinical heterogeneity in DLB. From this perspective, QSM-derived patterns may represent a promising tool for imaging-based phenotyping, potentially improving the characterization of disease heterogeneity and patient stratification in future studies and in clinical therapeutic trials.

This study is not exempt from limitations. First, our sample was relatively small and this might have affected statistical power limiting the emergence of subtle or subthreshold findings. This may also limit generalization of our findings. We acknowledge that there was a significant group effect for age, and this might have biased the results. To limit this bias, we included age as a covariate in all of our statistical models to limit the influence of confounding effects and improve accuracy, following an analytical strategy adopted in previous studies (Bhome et al., 2026; Dukart et al., 2011; Falahati et al., 2016). Another limitation is that we did not use a Real-Time Quaking Induced Conversion (RT-QuIC) assay for the detection of the level of alpha-synuclein aggregates in the cerebrospinal fluid of our participants. It should also be noted that, although QSM-derived magnetic susceptibility is widely used as a proxy for iron content, it reflects the combined contribution of multiple tissue components (e.g., iron, myelin, calcium, and microstructural properties). Therefore, while increased susceptibility is plausibly related to altered iron homeostasis – especially in deep gray matter – its interpretation in cortical regions should be approached with caution, also considering regional differences across brain lobes. Furthermore, we need to take into account the significant pathological heterogeneity among DLB patients and, in this study, some of our DLB patients also exhibited AD neuropathological changes, which could result in medial temporal atrophy (Oppedal et al., 2019). Our cross-sectional design does not allow us to determine spatiotemporal changes in iron and atrophy in dementia with Lewy Bodies. Longitudinal studies of other α-synucleinopathies and of patients in prodromal stages are needed to clarify the temporal and spatial trajectories of iron accumulation and their association with volume loss and cognitive decline. Future studies using larger and longitudinal samples, as well as studies with neuropathological validation, are needed to extend and increase the significance of the current findings. Finally, we acknowledge a methodological limitation. In this study a ROI approach was used to assess changes in magnetic susceptibility. This might have averaged across ROIs subtle changes in small areas that might have gone undetected in this sample. A voxel-based analytical approach, similar to that used in the study by Uchida et al (2019), would overcome this methodological limitation and would be desirable in future studies with a larger sample size. It is encouraging, however, that there are parallel findings (i.e. increased susceptibility in one subcortical area – namely the globus pallidus – and three cortical areas – precuneus, cuneus and insula) between our study and Uchida and colleagues' results, although these latter obtained in a sample of patients with PD. These converging findings suggest that our methodological approach had sufficient sensitivity to detect meaningful susceptibility changes in this DLB sample, although it cannot be ruled out that subtle regional changes might have been missed.

5. Conclusions

In conclusion, this study using a QSM technique provides novel insights into cortical and subcortical iron accumulation in patients with DLB. Increased iron overload was found especially in key subcortical structures involved in alpha-synucleinopathies, and these same regions were relevant to differentiate DLB early predominant phenotypes in our sample. Our findings suggest that QSM might represent a useful diagnostic biomarker to assess *in vivo* early changes reflective of neurodegeneration in DLB patients. Longitudinal studies with larger sample sizes are needed to understand the interplay between brain volumetric loss, iron accumulation, and clinical symptoms.

Funding

This study has been supported by the Italian Ministry of Health (#GR-2019–12369242) and by the "Ricerca Corrente" funding from the Italian Ministry of Health. MM and AV are supported by the National Recovery and Resilience Plan (NRRP), Mission 4 Component 2 Investment 1.3 – Call for tender No. 341 of 15/03/2022 of Italian Ministry of University and Research funded by the European Union –NextGen-erationEU, Project code PE0000006, Concession Decree No. 1553 of 11/10/2022 adopted by the Italian Ministry of University and Research, CUP D93C22000930002, "A multiscale integrated approach to the study of the nervous system in health and disease" (MNESYS).

CRediT authorship contribution statement

Elettra Capogna: Writing – original draft, Visualization, Methodology, Formal analysis, Conceptualization. **Greta Venturi:** Writing – original draft, Visualization, Methodology, Formal analysis, Conceptualization. **Lorenzo Motta:** Writing – review & editing, Methodology. **David Neil Manners:** Writing – review & editing, Methodology. **Davide Braghittoni:** Data curation. **Lucia Guidi:** Writing – review & editing, Data curation. **Luca Baldelli:** Writing – review & editing. **Giovanna Calandra-Buonaura:** Writing – review & editing. **Luisa Sambati:** Writing – review & editing, Data curation. **Annalena Venneri:** Writing – review & editing. **Caterina Tonon:** Writing – review & editing, Supervision, Funding acquisition, Conceptualization. **Micaela Mitolo:** Writing – review & editing, Supervision, Funding acquisition, Conceptualization. **Raffaele Lodi:** Writing – review & editing, Supervision, Funding acquisition, Conceptualization.

Declaration of competing interest

The authors declare that they have no known competing financial interests or personal relationships that could have appeared to influence the work reported in this paper.

Appendix A. Supplementary data

Supplementary data to this article can be found online at https://doi.org/10.1016/j.nicl.2026.104000.

Data availability

Data will be made available on request.

References

Abdelnour, C., Ferreira, D., van de Beek, M., Cedres, N., Oppedal, K., Cavallin, L., Blanc, F., Bousiges, O., Wahlund, L.-O., Pilotto, A., Padovani, A., Boada, M., Pagonabarraga, J., Kulisevsky, J., Aarsland, D., Lemstra, A.W., Westman, E., 2022. Parsing heterogeneity within dementia with Lewy bodies using clustering of biological, clinical, and demographic data. Alz. Res. Therapy 14, 14. https://doi.org/10.1186/s13195-021-00946-w.

Acosta-Cabronero, J., Cardenas-Blanco, A., Betts, M.J., Butryn, M., Valdes-Herrera, J.P., Galazky, I., Nestor, P.J., 2017. The whole-brain pattern of magnetic susceptibility perturbations in Parkinson's disease. Brain 140, 118–131. https://doi.org/10.1093/brain/aww278.

Barba, L., Abu-Rumeileh, S., Barthel, H., Massa, F., Foschi, M., Bellomo, G., Gaetani, L., Thal, D.R., Parnetti, L., Otto, M., 2024. Clinical and diagnostic implications of Alzheimer's disease copathology in Lewy body disease. Brain 147, 3325–3343. https://doi.org/10.1093/brain/awae203.

Benjamini, Y., Hochberg, Y., 1995. Controlling the false discovery rate: a practical and powerful approach to multiple testing. J. Roy. Stat. Soc.: Ser. B (Methodol.) 57, 289–300. https://doi.org/10.1111/j.2517-6161.1995.tb02031.x.

Beretta, L., Caminiti, S.P., Santangelo, R., Magnani, G., Ferrari-Pellegrini, F., Caffarra, P., Perani, D., 2019. Two distinct pathological substrates associated with MMSE-pentagons item deficit in DLB and AD. Neuropsychologia 133, 107174. https://doi.org/10.1016/j.neuropsychologia.2019.107174.

Beretta, L., Carli, G., Caffarra, P., Perani, D., 2022. Distinct brain dysfunctions underlying visuo-constructive deficit in DLB and AD. Brain Imaging Behav. 16, 532–537. https://doi.org/10.1007/s11682-021-00515-7.

Bhome, R., Thomas, G.E.C., Hannaway, N., Dobreva, I., Zarkali, A., Shmueli, K., Cole, J. H., Weil, R.S., 2026. Quantitative susceptibility mapping reveals differences between subtypes of Lewy body dementia. Brain 149, 1058–1069. https://doi.org/10.1093/brain/awaf325.

Biondetti, E., Karsa, A., Grussu, F., Battiston, M., Yiannakas, M.C., Thomas, D.L., Shmueli, K., 2022. Multi-echo quantitative susceptibility mapping: how to combine echoes for accuracy and precision at 3 Tesla. Magn. Reson. Med. 88, 2101–2116. https://doi.org/10.1002/mrm.29365.

Borghammer, P., Horsager, J., Andersen, K., Van Den Berge, N., Raunio, A., Murayama, S., Parkkinen, L., Myllykangas, L., 2021. Neuropathological evidence of body-first vs. brain-first Lewy body disease. Neurobiol. Dis. 161, 105557. https://doi.org/10.1016/j.nbd.2021.105557.

Caffarra, P., Vezzadini, G., Dieci, F., Zonato, F., 2002a. Una versione abbreviata del test di Stroop: dati normativi nella popolazione italiana.

Caffarra, P., Vezzadini, G., Dieci, F., Zonato, F., Venneri, A., 2002. Rey-Osterrieth complex figure: normative values in an italian population sample. Neurol. Sci. 22, 443–447. https://doi.org/10.1007/s100720200003.

Carlesimo, G.A., Caltagirone, C., Gainotti, G., 1996. The mental deterioration battery: normative data, diagnostic reliability and qualitative analyses of cognitive impairment. The group for the standardization of the mental deterioration battery. Eur. Neurol. 36, 378–384. https://doi.org/10.1159/000117297.

Chen, Q., Boeve, B.F., Forghanian-Arani, A., Senjem, M.L., Jack Jr., C.R., Przybelski, S.A., Lesnick, T.G., Kremers, W.K., Fields, J.A., Schwarz, C.G., Gunter, J.L., Trzasko, J.D., Graff-Radford, J., Savica, R., Knopman, D.S., Dickson, D.W., Ferman, T.J., Graff-Radford, N., Petersen, R.C., Kantarci, K., 2021. MRI quantitative susceptibility mapping of the substantia nigra as an early biomarker for Lewy body disease. J. Neuroimaging 31, 1020–1027. https://doi.org/10.1111/jon.12878.

Chen, Q., Chen, Y., Zhang, Y., Wang, F., Yu, H., Zhang, C., Jiang, Z., Luo, W., 2019. Iron deposition in Parkinson's disease by quantitative susceptibility mapping. BMC Neurosci. 20, 23. https://doi.org/10.1186/s12868-019-0505-9.

Chin, K.S., Yassi, N., Churilov, L., Masters, C.L., Watson, R., 2020. Prevalence and clinical associations of tau in Lewy body dementias: a systematic review and meta-analysis. Parkinsonism Relat. Disord. 80, 184–193. https://doi.org/10.1016/j.parkreldis.2020.09.030.

Colom-Cadena, M., Grau-Rivera, O., Planellas, L., Cerquera, C., Morenas, E., Helgueta, S., Muñoz, L., Kulisevsky, J., Martí, M.J., Tolosa, E., Clarimon, J., Lleó, A., Gelpi, E., 2017. Regional overlap of pathologies in lewy body disorders. J. Neuropathol. Exp. Neurol. 76, 216–224. https://doi.org/10.1093/jnen/nlx002.

Committee, Q.C.O., Bilgic, B., Costagli, M., Chan, K.-S., Duyn, J., Langkammer, C., Lee, J., Li, X., Liu, C., Marques, J.P., Milovic, C., Robinson, S.D., Schweser, F., Shmueli, K., Spincemaille, P., Straub, S., van Zijl, P., Wang, Y., Group, I.E.-M.T.P.S., 2024. Recommended implementation of quantitative susceptibility mapping for clinical research in the brain: a consensus of the ISMRM electro-magnetic tissue properties study group. Magn. Reson. Med. 91, 1834–1862. https://doi.org/10.1002/mrm.30006.

Costanzo, P., Orphanou, K., 2022. Performance, Transparency and Time. Feature selection to speed up the diagnosis of Parkinson's disease. https://doi.org/10.48550/arXiv.2206.03716.

Daugherty, A., Raz, N., 2013. Age-related differences in iron content of subcortical nuclei observed in vivo: a meta-analysis. Neuroimage 70, 113–121. https://doi.org/10.1016/j.neuroimage.2012.12.040.

De Marzi, R., Seppi, K., Högl, B., Müller, C., Scherfler, C., Stefani, A., Iranzo, A., Tolosa, E., Santamarìa, J., Gizewski, E., Schocke, M., Skalla, E., Kremser, C., Poewe, W., 2016. Loss of dorsolateral nigral hyperintensity on 3.0 tesla susceptibility-weighted imaging in idiopathic rapid eye movement sleep behavior disorder. Ann. Neurol. 79, 1026–1030. https://doi.org/10.1002/ana.24646.

Deistung, A., Schweser, F., Reichenbach, J.R., 2017. Overview of quantitative susceptibility mapping. NMR Biomed. 30, e3569.

Desikan, R.S., Ségonne, F., Fischl, B., Quinn, B.T., Dickerson, B.C., Blacker, D., Buckner, R.L., Dale, A.M., Maguire, R.P., Hyman, B.T., Albert, M.S., Killiany, R.J., 2006. An automated labeling system for subdividing the human cerebral cortex on MRI scans into gyral based regions of interest. Neuroimage 31, 968–980. https://doi.org/10.1016/j.neuroimage.2006.01.021.

Diaz-Galvan, P., Przybelski, S.A., Lesnick, T.G., Murray, M.E., Nguyen, A., Reichard, R.R., Dickson, D.W., Ono, D., Senjem, M.L., Schwarz, C.G., Gunter, J., Lowe, V., Forsberg, L.K., Fields, J.A., Savica, R., Graff-Radford, J., Ramanan, V.K., Jones, D., Botha, H., St Louis, E.K., Knopman, D., Day, G.S., Graff-Radford, N., Kremers, W., Petersen, R.C., Jack, C.R., Ferman, T.J., Boeve, B.F., Kantarci, K., 2025a. Substantia nigra iron deposition in lewy body disease: a magnetic resonance imaging and neuropathology study. Mov. Disord. https://doi.org/10.1002/mds.30265.

Diaz-Galvan, P., Przybelski, S.A., Lesnick, T.G., Nguyen, A.T., Murray, M.E., Reichard, R. R., Dickson, D.W., Ono, D., Schwarz, C.G., Senjem, M.L., Gunter, J.L., Lowe, V.J., Forsberg, L.K., Fields, J.A., Savica, R., Graff-Radford, J., Ramanan, V.K., Jones, D.T., Botha, H., Louis, E.K.S., Knopman, D.S., Day, G.S., Graff-Radford, N.R., Petersen, R. C., Clifford R Jack, J., Ferman, T.J., Boeve, B.F., Kantarci, K., 2025b. Substantia nigra iron deposition in Lewy body disease: an MRI quantitative susceptibility mapping and neuropathology study. Alzheimer's & Dementia 20, e091491. https://doi.org/10.1002/alz.091491.

Dixon, S.J., Stockwell, B.R., 2014. The role of iron and reactive oxygen species in cell death. Nat. Chem. Biol. 10, 9–17. https://doi.org/10.1038/nchembio.1416.

Du, G., Wang, E., Sica, C., Chen, H., De Jesus, S., Lewis, M.M., Kong, L., Connor, J., Mailman, R.B., Huang, X., 2022. Dynamics of nigral iron accumulation in parkinson's disease: from diagnosis to late stage. Mov. Disord. 37, 1654–1662. https://doi.org/10.1002/mds.29062.

Dukart, J., Schroeter, M.L., Mueller, K., Alzheimer's Disease Neuroimaging Initiative, 2011. Age correction in dementia–matching to a healthy brain. PLoS One 6, e22193. https://doi.org/10.1371/journal.pone.0022193.

Duyn, J.H., Schenck, J., 2017. Contributions to magnetic susceptibility of brain tissue. NMR Biomed. 30. https://doi.org/10.1002/nbm.3546.

Elder, G.J., Mactier, K., Colloby, S.J., Watson, R., Blamire, A.M., O'Brien, J.T., Taylor, J.-P., 2017. The influence of hippocampal atrophy on the cognitive phenotype of dementia with Lewy bodies. Int. J. Geriatr. Psychiatry 32, 1182–1189. https://doi.org/10.1002/gps.4719.

Falahati, F., Ferreira, D., Soininen, H., Mecocci, P., Vellas, B., Tsolaki, M., Kłoszewska, I., Lovestone, S., Eriksdotter, M., Wahlund, L.-O., Simmons, A., Westman, E., AddNeuroMed consortium and the Alzheimer's Disease Neuroimaging Initiative, 2016. The effect of age correction on multivariate classification in alzheimer's disease, with a focus on the characteristics of incorrectly and correctly classified subjects. Brain Topogr. 29, 296–307. https://doi.org/10.1007/s10548-015-0455-1.

Ferman, T.J., Aoki, N., Boeve, B.F., Aakre, J.A., Kantarci, K., Graff-Radford, J., Parisi, J. E., Van Gerpen, J.A., Graff-Radford, N.R., Uitti, R.J., Pedraza, O., Murray, M.E., Wszolek, Z.K., Reichard, R.R., Fields, J.A., Ross, O.A., Knopman, D.S., Petersen, R.C., Dickson, D.W., 2020. Subtypes of dementia with Lewy bodies are associated with

α-synuclein and tau distribution. Neurology 95, e155–e165. https://doi.org/10.1212/WNL.0000000000009763.
Ferracuti, S., Cannoni, E., Hufty, A.M., 2000. Adattamento italiano di ":Contributi per un assessment neuropsicologico. Un manuale clinico" di A. L. Benton, A. B. Silvan, K. DeS. Hamster, N. R. Varney, O. Spreenet al. ITA.
Ferreira, D., Nedelska, Z., Graff-Radford, J., Przybelski, S.A., Lesnick, T.G., Schwarz, C. G., Botha, H., Senjem, M.L., Fields, J.A., Knopman, D.S., Savica, R., Ferman, T.J., Graff-Radford, N.R., Lowe, V.J., Jack, C.R., Petersen, R.C., Lemstra, A.W., van de Beek, M., Barkhof, F., Blanc, F., Loureiro de Sousa, P., Philippi, N., Cretin, B., Demuynck, C., Hort, J., Oppedal, K., Boeve, B.F., Aarsland, D., Westman, E., Kantarci, K., 2021. Cerebrovascular disease, neurodegeneration, and clinical phenotype in dementia with Lewy bodies. Neurobiol. Aging 105, 252–261. https://doi.org/10.1016/j.neurobiolaging.2021.04.029.
Ferreira, D., Przybelski, S.A., Lesnick, T.G., Lemstra, A.W., Londos, E., Blanc, F., Nedelska, Z., Schwarz, C.G., Graff-Radford, J., Senjem, M.L., Fields, J.A., Knopman, D.S., Savica, R., Ferman, T.J., Graff-Radford, N.R., Lowe, V.J., Jack, C.R., Petersen, R.C., Mollenhauer, B., Garcia-Ptacek, S., Abdelnour, C., Hort, J., Bonanni, L., Oppedal, K., Kramberger, M.G., Boeve, B.F., Aarsland, D., Westman, E., Kantarci, K., 2020. β-Amyloid and tau biomarkers and clinical phenotype in dementia with Lewy bodies. Neurology 95, e3257–e3268. https://doi.org/10.1212/WNL.0000000000010943.
Ffytche, D.H., Howard, R.J., Brammer, M.J., David, A., Woodruff, P., Williams, S., 1998. The anatomy of conscious vision: an fMRI study of visual hallucinations. Nat. Neurosci. 1, 738–742. https://doi.org/10.1038/3738.
Fischl, B., Salat, D.H., Busa, E., Albert, M., Dieterich, M., Haselgrove, C., van der Kouwe, A., Killiany, R., Kennedy, D., Klaveness, S., Montillo, A., Makris, N., Rosen, B., Dale, A.M., 2002. Whole brain segmentation: automated labeling of neuroanatomical structures in the human brain. Neuron 33, 341–355. https://doi.org/10.1016/S0896-6273(02)00569-X.
Fiscone, C., Rundo, L., Lugaresi, A., Manners, D.N., Allinson, K., Baldin, E., Vornetti, G., Lodi, R., Tonon, C., Testa, C., Castelli, M., Zaccagna, F., 2023. Assessing robustness of quantitative susceptibility-based MRI radiomic features in patients with multiple sclerosis. Sci. Rep. 13, 16239. https://doi.org/10.1038/s41598-023-42914-4.
Fiscone, C., Sighinolfi, G., Manners, D.N., Motta, L., Venturi, G., Panzera, I., Zaccagna, F., Rundo, L., Lugaresi, A., Lodi, R., Tonon, C., Castelli, M., 2024. Multiparametric MRI dataset for susceptibility-based radiomic feature extraction and analysis. Sci. Data 11, 575. https://doi.org/10.1038/s41597-024-03418-6.
Fu, X., Deng, W., Cui, X., Zhou, X., Song, W., Pan, M., Chi, X., Xu, J., Jiang, Y., Wang, Q., Xu, Y., 2021. Time-specific pattern of iron deposition in different regions in parkinson's disease measured by quantitative susceptibility mapping. Front. Neurol. 12. https://doi.org/10.3389/fneur.2021.631210.
Galbiati, A., Verga, L., Giora, E., Zucconi, M., Ferini-Strambi, L., 2019. The risk of neurodegeneration in REM sleep behavior disorder: a systematic review and meta-analysis of longitudinal studies. Sleep Med. Rev. 43, 37–46. https://doi.org/10.1016/j.smrv.2018.09.008.
Ghassaban, K., He, N., Sethi, S.K., Huang, P., Chen, S., Yan, F., Haacke, E.M., 2019. Regional high iron in the substantia nigra differentiates parkinson's disease patients from healthy controls. Front. Aging Neurosci. 11, 106. https://doi.org/10.3389/fnagi.2019.00106.
Haider, L., Simeonidou, C., Steinberger, G., Hametner, S., Grigoriadis, N., Deretzi, G., Kovacs, G.G., Kutzelnigg, A., Lassmann, H., Frischer, J.M., 2014. Multiple sclerosis deep grey matter: the relation between demyelination, neurodegeneration, inflammation and iron. J. Neurol. Neurosurg. Psychiatry 85, 1386–1395. https://doi.org/10.1136/jnnp-2014-307712.
He, N., Ling, H., Ding, B., Huang, J., Zhang, Y., Zhang, Z., Liu, C., Chen, K., Yan, F., 2015. Region-specific disturbed iron distribution in early idiopathic Parkinson's disease measured by quantitative susceptibility mapping. Hum. Brain Mapp. 36, 4407–4420. https://doi.org/10.1002/hbm.22928.
Horsager, J., Borghammer, P., 2024. Brain-first vs. body-first Parkinson's disease: an update on recent evidence. Parkinsonism Relat. Disord. 122, 106101. https://doi.org/10.1016/j.parkreldis.2024.106101.
Iglesias, J.E., Van Leemput, K., Bhatt, P., Casillas, C., Dutt, S., Schuff, N., Truran-Sacrey, D., Boxer, A., Fischl, B., Alzheimer's Disease Neuroimaging Initiative, 2015. Bayesian segmentation of brainstem structures in MRI. Neuroimage 113, 184–195. https://doi.org/10.1016/j.neuroimage.2015.02.065.
Inguanzo, A., Poulakis, K., Mohanty, R., Schwarz, C.G., Przybelski, S.A., Diaz-Galvan, P., Lowe, V.J., Boeve, B.F., Lemstra, A.W., van de Beek, M., van der Flier, W., Barkhof, F., Blanc, F., Loureiro de Sousa, P., Philippi, N., Cretin, B., Demuynck, C., Nedelska, Z., Hort, J., Segura, B., Junque, C., Oppedal, K., Aarsland, D., Westman, E., Kantarci, K., Ferreira, D., 2023. MRI data-driven clustering reveals different subtypes of Dementia with Lewy Bodies. NPJ Parkinsons. Dis. 9, 5. https://doi.org/10.1038/s41531-023-00448-6.
Irwin, D.J., Grossman, M., Weintraub, D., Hurtig, H.I., Duda, J.E., Xie, S.X., Lee, E.B., Van Deerlin, V.M., Lopez, O.L., Kofler, J.K., Nelson, P.T., Jicha, G.A., Woltjer, R., Quinn, J.F., Kaye, J., Leverenz, J.B., Tsuang, D., Longfellow, K., Yearout, D., Kukull, W., Keene, C.D., Montine, T.J., Zabetian, C.P., Trojanowski, J.Q., 2017. Neuropathological and genetic correlates of survival and dementia onset in synucleinopathies: a retrospective analysis. Lancet Neurol. 16, 55–65. https://doi.org/10.1016/S1474-4422(16)30291-5.
Jellinger, K.A., 2009. A critical evaluation of current staging of α-synuclein pathology in Lewy body disorders. Biochim. et Biophys. Acta (BBA) – Mol. Basis Disease, Parkinson's Disease 1792, 730–740. https://doi.org/10.1016/j.bbadis.2008.07.006.
Jenkinson, M., Smith, S., 2001. A global optimisation method for robust affine registration of brain images. Med. Image Anal. 5, 143–156. https://doi.org/10.1016/S1361-8415(01)00036-6.
Johns, M.W., 1991. A new method for measuring daytime sleepiness: the Epworth sleepiness scale. Sleep 14, 540–545. https://doi.org/10.1093/sleep/14.6.540.
Joza, S., Hu, M.T., Jung, K.-Y., Kunz, D., Stefani, A., Dušek, P., Terzaghi, M., Arnaldi, D., Videnovic, A., Schiess, M.C., Hermann, W., Lee, J.-Y., Ferini-Strambi, L., Lewis, S.J. G., Leclair-Visonneau, L., Oertel, W.H., Antelmi, E., Sixel-Döring, F., Cochen De Cock, V., Liguori, C., Liu, J., Provini, F., Puligheddu, M., Nicoletti, A., Bassetti, C.L. A., Bušková, J., Dauvilliers, Y., Ferri, R., Montplaisir, J.Y., Lawton, M., Kim, H.-J., Bes, F., Högl, B., Šonka, K., Fiamingo, G., Mattioli, P., Lavadia, M.L., Suescun, J., Woo, K.A., Marelli, S., Martens, K.E., Janzen, A., Plazzi, G., Mollenhauer, B., Fernandes, M., Li, Y., Cortelli, P., Figorilli, M., Cicero, C.E., Schaefer, C., Guiraud, L., Lanza, G., Gagnon, J.-F., Sunwoo, J.-S., Ibrahim, A., Girtler, N., Trenkwalder, C., Baldelli, L., Pelletier, A., Postuma, R.B., International REM Sleep Behavior Disorder Study Group, 2023. Progression of clinical markers in prodromal Parkinson's disease and dementia with Lewy bodies: a multicentre study. Brain 146, 3258–3272. https://doi.org/10.1093/brain/awad072.
Keuken, M.C., Forstmann, B.U., 2015. A probabilistic atlas of the basal ganglia using 7 T MRI. Data Brief 4, 577–582. https://doi.org/10.1016/j.dib.2015.07.028.
Khadhraoui, E., Müller, S.J., Hansen, N., Riedel, C.H., Langer, P., Timäeus, C., Wiltfang, J., Bouter, C., Lange, C., Ernst, M., 2022. Manual and automated analysis of atrophy patterns in dementia with Lewy bodies on MRI. BMC Neurol. 22, 114. https://doi.org/10.1186/s12883-022-02642-0.
Kiersnowski, O.C., Mattioli, P., Argenti, L., Avanzino, L., Calizzano, F., Diociasi, A., Falcitano, L., Liu, C., Losa, M., Massa, F., Morbelli, S., Orso, B., Pelosin, E., Raffa, S., Pardini, M., Arnaldi, D., Roccatagliata, L., Costagli, M., 2025. Magnetic susceptibility components reveal different aspects of neurodegeneration in alpha-synucleinopathies. Sci. Rep. 15, 4186. https://doi.org/10.1038/s41598-024-83593-z.
Kostka, M., Högen, T., Danzer, K.M., Levin, J., Habeck, M., Wirth, A., Wagner, R., Glabe, C.G., Finger, S., Heinzelmann, U., Garidel, P., Duan, W., Ross, C.A., Kretzschmar, H., Giese, A., 2008. Single particle characterization of iron-induced pore-forming alpha-synuclein oligomers. J. Biol. Chem. 283, 10992–11003. https://doi.org/10.1074/jbc.M709634200.
Lancione, M., Donatelli, G., Del Prete, E., Campese, N., Frosini, D., Cencini, M., Costagli, M., Biagi, L., Lucchi, G., Tosetti, M., Godani, M., Arnaldi, D., Terzaghi, M., Provini, F., Pacchetti, C., Cortelli, P., Bonanni, E., Ceravolo, R., Cosottini, M., 2022. Evaluation of iron overload in nigrosome 1 via quantitative susceptibility mapping as a progression biomarker in prodromal stages of synucleinopathies. Neuroimage 260, 119454. https://doi.org/10.1016/j.neuroimage.2022.119454.
Langkammer, C., Pirpamer, L., Seiler, S., Deistung, A., Schweser, F., Franthal, S., Homayoon, N., Katschnig-Winter, P., Koegl-Wallner, M., Pendl, T., Stoegerer, E.M., Wenzel, K., Fazekas, F., Ropele, S., Reichenbach, J.R., Schmidt, R., Schwingenschuh, P., 2016. Quantitative susceptibility mapping in parkinson's disease. PLoS One 11, e0162460. https://doi.org/10.1371/journal.pone.0162460.
Langkammer, C., Schweser, F., Krebs, N., Deistung, A., Goessler, W., Scheurer, E., Sommer, K., Reishofer, G., Yen, K., Fazekas, F., Ropele, S., Reichenbach, J.R., 2012. Quantitative susceptibility mapping (QSM) as a means to measure brain iron? A post mortem validation study. Neuroimage 62, 1593–1599. https://doi.org/10.1016/j.neuroimage.2012.05.049.
Levi, S., Ripamonti, M., Moro, A.S., Cozzi, A., 2024. Iron imbalance in neurodegeneration. Mol. Psychiatry 29, 1139–1152. https://doi.org/10.1038/s41380-023-02399-z.
Levin, J., Högen, T., Hillmer, A.S., Bader, B., Schmidt, F., Kamp, F., Kretzschmar, H.A., Bötzel, K., Giese, A., 2011. Generation of ferric iron links oxidative stress to α-synuclein oligomer formation. J. Parkinsons Dis. 1, 205–216. https://doi.org/10.3233/JPD-2011-11040.
Li, W., Wang, N., Yu, F., Han, H., Cao, W., Romero, R., Tantiwongkosi, B., Duong, T.Q., Liu, C., 2015. A method for estimating and removing streaking artifacts in quantitative susceptibility mapping. Neuroimage 108, 111–122. https://doi.org/10.1016/j.neuroimage.2014.12.043.
Li, W., Wu, B., Liu, C., 2011. Quantitative susceptibility mapping of human brain reflects spatial variation in tissue composition. Neuroimage 55, 1645–1656. https://doi.org/10.1016/j.neuroimage.2010.11.088.
Madden, D.J., Merenstein, J.L., 2023. Quantitative susceptibility mapping of brain iron in healthy aging and cognition. Neuroimage 282, 120401. https://doi.org/10.1016/j.neuroimage.2023.120401.
Masaldan, S., Bush, A.I., Devos, D., Rolland, A.S., Moreau, C., 2019. Striking while the iron is hot: Iron metabolism and ferroptosis in neurodegeneration. Free Radical Biology and Medicine, Iron as Soul of Life on Earth Revisited: from Chemical Reaction, Ferroptosis to Therapeutics 133, 221–233. https://doi.org/10.1016/j.freeradbiomed.2018.09.033.
McGregor, M.M., Nelson, A.B., 2019. Circuit mechanisms of parkinson's disease. Neuron 101, 1042–1056. https://doi.org/10.1016/j.neuron.2019.03.004.
McKeith, I.G., Boeve, B.F., Dickson, D.W., Halliday, G., Taylor, J.-P., Weintraub, D., Aarsland, D., Galvin, J., Attems, J., Ballard, C.G., Bayston, A., Beach, T.G., Blanc, F., Bohnen, N., Bonanni, L., Bras, J., Brundin, P., Burn, D., Chen-Plotkin, A., Duda, J.E., El-Agnaf, O., Feldman, H., Ferman, T.J., Ffytche, D., Fujishiro, H., Galasko, D., Goldman, J.G., Gomperts, S.N., Graff-Radford, N.R., Honig, L.S., Iranzo, A., Kantarci, K., Kaufer, D., Kukull, W., Lee, V.M.Y., Leverenz, J.B., Lewis, S., Lippa, C., Lunde, A., Masellis, M., Masliah, E., McLean, P., Mollenhauer, B., Montine, T.J., Moreno, E., Mori, E., Murray, M., O'Brien, J.T., Orimo, S., Postuma, R.B., Ramaswamy, S., Ross, O.A., Salmon, D.P., Singleton, A., Taylor, A., Thomas, A., Tiraboschi, P., Toledo, J.B., Trojanowski, J.Q., Tsuang, D., Walker, Z., Yamada, M., Kosaka, K., 2017. Diagnosis and management of dementia with Lewy bodies. Neurology 89, 88–100. https://doi.org/10.1212/WNL.0000000000004058.
Miglis, M.G., Adler, C.H., Antelmi, E., Arnaldi, D., Baldelli, L., Boeve, B.F., Cesari, M., Dall'Antonia, I., Diederich, N.J., Doppler, K., Dušek, P., Ferri, R., Gagnon, J.-F., Gan-

Or, Z., Hermann, W., Högl, B., Hu, M.T., Iranzo, A., Janzen, A., Kuzkina, A., Lee, J.-Y., Leenders, K.L., Lewis, S.J.G., Liguori, C., Liu, J., Lo, C., Ehgoetz Martens, K.A., Nepozitek, J., Plazzi, G., Provini, F., Puligheddu, M., Rolinski, M., Rusz, J., Stefani, A., Summers, R.L.S., Yoo, D., Zitser, J., Oertel, W.H., 2021. Biomarkers of conversion to α-synucleinopathy in isolated rapid-eye-movement sleep behaviour disorder. Lancet Neurol. 20, 671–684. https://doi.org/10.1016/S1474-4422(21)00176-9.

Mohammadi, S., Ghaderi, S., 2024. Parkinson's disease and Parkinsonism syndromes: evaluating iron deposition in the putamen using magnetic susceptibility MRI techniques - a systematic review and literature analysis. Heliyon 10. https://doi.org/10.1016/j.heliyon.2024.e27950.

Monaco, M., Costa, A., Caltagirone, C., Carlesimo, G.A., 2013. Forward and backward span for verbal and visuo-spatial data: standardization and normative data from an italian adult population. Neurol. Sci. 34, 749–754. https://doi.org/10.1007/s10072-012-1130-x.

Moon, Y., Han, S.-H., Moon, W.-J., 2016. Patterns of brain iron accumulation in vascular dementia and alzheimer's dementia using quantitative susceptibility mapping imaging. J. Alzheimer's Dis. 51, 737–745. https://doi.org/10.3233/JAD-151037.

Morenas-Rodríguez, E., Sala, I., Subirana, A., Pascual-Goñi, E., Sánchez-Saudinós, M.B., Alcolea, D., Illán-Gala, I., Carmona-Iragui, M., Ribosa-Nogué, R., Camacho, V., Blesa, R., Fortea, J., Lleó, A., 2018. Clinical subtypes of dementia with lewy bodies based on the initial clinical presentation. J. Alzheimers Dis. 64, 505–513. https://doi.org/10.3233/JAD-180167.

Morris, G., Berk, M., Carvalho, A.F., Maes, M., Walker, A.J., Puri, B.K., 2018. Why should neuroscientists worry about iron? the emerging role of ferroptosis in the pathophysiology of neuroprogressive diseases. Behav. Brain Res. 341, 154–175. https://doi.org/10.1016/j.bbr.2017.12.036.

Ndayisaba, A., Kaindlstorfer, C., Wenning, G.K., 2019. Iron in Neurodegeneration - cause or consequence? Front. Neurosci. 13, 180. https://doi.org/10.3389/fnins.2019.00180.

Nepozitek, J., Varga, Z., Dostalova, S., Perinova, P., Keller, J., Robinson, S., Ibarburu, V., Prihodova, I., Bezdicek, O., Ruzicka, E., Sonka, K., Dusek, P., 2023. Magnetic susceptibility changes in the brainstem reflect REM sleep without atonia severity in isolated REM sleep behavior disorder. NPJ Parkinsons Dis. 9, 112. https://doi.org/10.1038/s41531-023-00557-2.

Oppedal, K., Ferreira, D., Cavallin, L., Lemstra, A.W., Ten Kate, M., Padovani, A., Rektorova, I., Bonanni, L., Wahlund, L.-O., Engedal, K., Nobili, F., Kramberger, M., Taylor, J.-P., Hort, J., Snædal, J., Blanc, F., Walker, Z., Antonini, A., Westman, E., Aarsland, D., Alzheimer's Disease Neuroimaging Initiative, 2019. A signature pattern of cortical atrophy in dementia with Lewy bodies: a study on 333 patients from the European DLB consortium. Alzheimers Dement. 15, 400–409. https://doi.org/10.1016/j.jalz.2018.09.011.

Outeiro, T.F., Koss, D.J., Erskine, D., Walker, L., Kurzawa-Akanbi, M., Burn, D., Donaghy, P., Morris, C., Taylor, J.-P., Thomas, A., Attems, J., McKeith, I., 2019. Dementia with Lewy bodies: an update and outlook. Mol. Neurodegener. 14, 5. https://doi.org/10.1186/s13024-019-0306-8.

Patel, D., Xu, C., Nagarajan, S., Liu, Z., Hemphill, W.O., Shi, R., Uversky, V.N., Caldwell, G.A., Caldwell, K.A., Witt, S.N., 2018. Alpha-synuclein inhibits Snx3-retromer-mediated retrograde recycling of iron transporters in S. cerevisiae and C. elegans models of Parkinson's disease. Hum. Mol. Genet. 27, 1514–1532. https://doi.org/10.1093/hmg/ddy059.

Peng, Y., Wang, C., Xu, H.H., Liu, Y.-N., Zhou, F., 2010. Binding of alpha-synuclein with Fe(III) and with Fe(II) and biological implications of the resultant complexes. J. Inorg. Biochem. 104, 365–370. https://doi.org/10.1016/j.jinorgbio.2009.11.005.

Ravanfar, P., Loi, S.M., Syeda, W.T., Van Rheenen, T.E., Bush, A.I., Desmond, P., Cropley, V.L., Lane, D.J.R., Opazo, C.M., Moffat, B.A., Velakoulis, D., Pantelis, C., 2021. Systematic review: quantitative susceptibility mapping (QSM) of brain iron profile in neurodegenerative diseases. Front. Neurosci. 15, 618435. https://doi.org/10.3389/fnins.2021.618435.

Rouault, T.A., 2013. Iron metabolism in the CNS: implications for neurodegenerative diseases. Nat. Rev. Neurosci. 14, 551–564. https://doi.org/10.1038/nrn3453.

Schweser, F., Deistung, A., Lehr, B.W., Reichenbach, J.R., 2011. Quantitative imaging of intrinsic magnetic tissue properties using MRI signal phase: an approach to in vivo brain iron metabolism? Neuroimage 54, 2789–2807. https://doi.org/10.1016/j.neuroimage.2010.10.070.

Shahmaei, V., Faeghi, F., Mohammdbeigi, A., Hashemi, H., Ashrafi, F., 2019. Evaluation of iron deposition in brain basal ganglia of patients with Parkinson's disease using quantitative susceptibility mapping. Eur. J. Radiol. Open 6, 169–174. https://doi.org/10.1016/j.ejro.2019.04.005.

Straub, S., Schneider, T.M., Emmerich, J., Freitag, M.T., Ziener, C.H., Schlemmer, H.-P., Ladd, M.E., Laun, F.B., 2017. Suitable reference tissues for quantitative susceptibility mapping of the brain. Magn. Reson. Med. 78, 204–214. https://doi.org/10.1002/mrm.26369.

Sun, J., Lai, Z., Ma, J., Gao, L., Chen, M., Chen, J., Fang, J., Fan, Y., Bao, Y., Zhang, D., Chan, P., Yang, Q., Ye, C., Wu, T., Ma, T., 2020. Quantitative evaluation of iron content in idiopathic rapid eye movement sleep behavior disorder. Mov. Disord. 35, 478–485. https://doi.org/10.1002/mds.27929.

Thomas, G.E.C., Leyland, L.A., Schrag, A.-E., Lees, A.J., Acosta-Cabronero, J., Weil, R.S., 2020. Brain iron deposition is linked with cognitive severity in Parkinson's disease. J. Neurol. Neurosurg. Psychiatry 91, 418–425. https://doi.org/10.1136/jnnp-2019-322042.

Thomas, L.O., Boyko, O.B., Anthony, D.C., Burger, P.C., 1993. MR detection of brain iron. Am. J. Neuroradiol. 14, 1043–1048.

Toledo, J.B., Gopal, P., Raible, K., Irwin, D.J., Brettschneider, J., Sedor, S., Waits, K., Boluda, S., Grossman, M., Van Deerlin, V.M., Lee, E.B., Arnold, S.E., Duda, J.E., Hurtig, H., Lee, V.-M.-Y., Adler, C.H., Beach, T.G., Trojanowski, J.Q., 2016. Pathological α-synuclein distribution in subjects with coincident Alzheimer's and Lewy body pathology. Acta Neuropathol. 131, 393–409. https://doi.org/10.1007/s00401-015-1526-9.

Uchida, Y., Kan, H., Sakurai, K., Arai, N., Kato, D., Kawashima, S., Ueki, Y., Matsukawa, N., 2019. Voxel-based quantitative susceptibility mapping in Parkinson's disease with mild cognitive impairment. Mov. Disord. 34, 1164–1173. https://doi.org/10.1002/mds.27717.

Uchida, Y., Kan, H., Sakurai, K., Inui, S., Kobayashi, S., Akagawa, Y., Shibuya, K., Ueki, Y., Matsukawa, N., 2020. Magnetic susceptibility associates with dopaminergic deficits and cognition in parkinson's disease. Mov. Disord. 35, 1396–1405. https://doi.org/10.1002/mds.28077.

Vann Jones, S.A., O'Brien, J.T., 2014. The prevalence and incidence of dementia with Lewy bodies: a systematic review of population and clinical studies. Psychol. Med. 44, 673–683. https://doi.org/10.1017/S0033291713000494.

Varga, Z., Keller, J., Robinson, S.D., Serranova, T., Nepozitek, J., Zogala, D., Trnka, J., Ruzicka, E., Sonka, K., Dusek, P., 2024. Whole brain pattern of iron accumulation in REM sleep behavior disorder. Hum. Brain Mapp. 45, e26675. https://doi.org/10.1002/hbm.26675.

Wang, Y., Liu, T., 2015. Quantitative susceptibility mapping (QSM): Decoding MRI data for a tissue magnetic biomarker. Magn. Reson. Med. 73, 82–101. https://doi.org/10.1002/mrm.25358.

Ward, R.J., Zucca, F.A., Duyn, J.H., Crichton, R.R., Zecca, L., 2014. The role of iron in brain ageing and neurodegenerative disorders. Lancet Neurol. 13, 1045–1060. https://doi.org/10.1016/S1474-4422(14)70117-6.

Warrington, E.K., James, M., 1991. The Visual Object and Space Perception Battery. VOSP. Pearson.

Weintraub, D., Dietz, N., Duda, J.E., Wolk, D.A., Doshi, J., Xie, S.X., Davatzikos, C., Clark, C.M., Siderowf, A., 2012. Alzheimer's disease pattern of brain atrophy predicts cognitive decline in Parkinson's disease. Brain 135, 170–180. https://doi.org/10.1093/brain/awr277.

Wiggermann, V., 2023. Chapter 3 - Iron imaging in neuroinflammation. In: Laule, C., Port, J.D. (Eds.), Advances in Magnetic Resonance Technology and Applications, Imaging Neuroinflammation. Academic Press, pp. 51–78, 10.1016/B978-0-323-91771-1.00013-7.

Yao, J., Morrison, M.A., Jakary, A., Avadiappan, S., Chen, Y., Luitjens, J., Glueck, J., Driscoll, T., Geschwind, M.D., Nelson, A.B., Villanueva-Meyer, J.E., Hess, C.P., Lupo, J.M., 2023. Comparison of quantitative susceptibility mapping methods for iron-sensitive susceptibility imaging at 7T: an evaluation in healthy subjects and patients with Huntington's disease. Neuroimage 265, 119788. https://doi.org/10.1016/j.neuroimage.2022.119788.

Zarino, B., Crespi, M., Launi, M., Casarotti, A., 2014. A new standardization of semantic verbal fluency test. Neurol. Sci. 35, 1405–1411. https://doi.org/10.1007/s10072-014-1729-1.

Zeng, W., Cai, J., Zhang, L., Peng, Q., 2024. Iron Deposition in Parkinson's Disease: a Mini-Review. Cell. Mol. Neurobiol. 44, 26. https://doi.org/10.1007/s10571-024-01459-4.

Zoetmulder, M., Nikolic, M., Biernat, H., Korbo, L., Friberg, L., Jennum, P., 2016. Increased motor activity during rem sleep is linked with dopamine function in idiopathic REM sleep behavior disorder and parkinson disease. J. Clin. Sleep Med.: JCSM : Official Publ. Am. Acad. Sleep Med. 12, 895. https://doi.org/10.5664/jcsm.5896.

Zorzi, G., Cecchin, D., Bussè, C., Perini, G., Corbetta, M., Cagnin, A., 2021. Changes of metabolic connectivity in dementia with lewy bodies with visual hallucinations: a 18F-fluorodeoxyglucose positron emission tomography/magnetic resonance study. Brain Connect. 11, 518–528. https://doi.org/10.1089/brain.2020.0988.